remote sensing

MDPI

Article

An Approach to Improve the Spatial Resolution and Accuracy of AMSR2 Passive Microwave Snow Depth Product Using Machine Learning in Northeast China

Yanlin Wei [1,2], Xiaofeng Li [1,3,*], Li Li [4], Lingjia Gu [5], Xingming Zheng [1], Tao Jiang [1] and Xiaojie Li [1]

1 Northeast Institute of Geography and Agroecology, Chinese Academy of Sciences, Changchun 130102, China; weiyl18@mails.jlu.edu.cn (Y.W.); zhengxingming@iga.ac.cn (X.Z.); jiangtao@iga.ac.cn (T.J.); lixiaojie@iga.ac.cn (X.L.)
2 University of Chinese Academy of Sciences, Beijing 100049, China
3 Changchun Jingyuetan Remote Sensing Experiment Site, Chinese Academy of Sciences, Changchun 130102, China
4 College of Science, Qiqihar University, Qiqihar 161006, China; lili19762001@163.com
5 College of Electronic Science & Engineering, Jilin University, Changchun 130012, China; gulingjia@jlu.edu.cn
* Correspondence: lixiaofeng@iga.ac.cn

Abstract: Snow cover plays a highly critical role in the global water cycle and energy exchange. Accurate snow depth (SD) data are important for research on hydrologic processes, climate change, and natural disaster prediction. However, existing passive microwave (PMW) SD products have high uncertainty in Northeast China owing to their coarse spatial resolution. Surface environment parameters should also be considered to reduce errors in existing SD products. Otherwise, it is difficult to accurately capture snow spatiotemporal variations, especially in a complex environment (e.g., mountain or forests areas). To improve the inversion accuracy and spatial resolution of existing SD products in Northeast China, a multifactor SD downscaling model was developed by combining PMW SD data from the AMSR2 sensor, optical snow cover extent data, and surface environmental parameters to produce fine scale (500 m $\times$ 500 m) and high precision SD data. Validations at 98 ground meteorological stations show that the developed model greatly improved the spatial resolution and inversion accuracy of the raw AMSR2 SD product; its root-mean-square error (RMSE) reduced from 26.15 cm of the raw product to 7.58 cm, and the correlation coefficient (R) increased from 0.39 to 0.53. For other SD products (WESTDC and FY), the multifactor SD downscaling model still has good applicability, it could further improve the performance of the WESTDC and FY SD products in time and space and achieve better inversion accuracy than raw SD products. Furthermore, the proposed model exhibited good agreement with the observed SD data in a field quadrat (3 km $\times$ 2 km) within the fine scale, with an error ranging between -2 and 2 cm. Compared with the existing downscaling methods, the proposed model presented the best performance.

Keywords: snow depth; Northeast China; downscaling model; passive microwave; machine learning

Citation: Wei, Y.; Li, X.; Li, L.; Gu, L.; Zheng, X.; Jiang, T.; Li, X. An Approach to Improve the Spatial Resolution and Accuracy of AMSR2 Passive Microwave Snow Depth Product Using Machine Learning in Northeast China. *Remote Sens.* **2022**, *14*, 1480. https://doi.org/10.3390/rs14061480

Academic Editor: Sang-Eun Park

Received: 12 February 2022
Accepted: 15 March 2022
Published: 18 March 2022

1. Introduction

Snow cover is a key part of the global water cycle and climate system [1], and it greatly influences the surface temperature and radiation budget at a local and global scale owing to its high reflectivity [2–4]. Furthermore, snow depth (SD) is one of the most crucial elements for climate change, hydrological process research, and weather forecasting. Therefore, reliable SD estimation is important for performing significative statistics on the trends and variability in these studies [5–8]. As one of the major snow-covered regions in China, Northeast China has sufficient snow resources; the changes of seasonal snow are directly related to global climate change [9,10]. Moreover, Northeast China is also an essential agricultural base in China. Snowmelt is a key supplementary water source for soil moisture and crop growth in the spring [11,12]. Therefore, studying snow is necessary for monitoring climate environment changes and agricultural development in Northeast China.

The remote sensing technique is one of the most efficient methods for detecting seasonal snow cover extent on the regional and even the global scale [3]. Compared with optical remote sensing, passive microwave (PMW) remote sensing does not depend on sunlight and weather conditions [9] and can penetrate snow layers and interact with the snow particles; therefore, it is the most effective method for SD inversion [3,7]. In addition, spaceborne PMW sensors have been developed since the 1970s, offering strong data resources for studying seasonal snow change [13,14]. The emitted radiation from the earth's surface decreases as the snow thickness increases during snowpack accumulation [15]. To this end, diverse empirical SD inversion algorithms have been presented over the past several decades. The most commonly used SD retrieval algorithms were based on empirical relationships between SD and PMW brightness temperature difference [13,16,17]. However, many studies have shown that these empirical algorithms generate large uncertainties in different regions owing to the empirical constants that are fixed [18–20]. Although more advanced methods, such as theoretical snow layer radiative transfer models [21,22], were proposed and produced more reliable results compared with the empirical SD inversion algorithms, they largely depended on prior knowledge of the model parameters. This fact is not favourable to large-scale SD information inversion. [23,24]. A data assimilation technique for improving the accuracy of SD assessments was proposed by Pulliainen in 2006, and produced daily snow water equivalent (SWE) dataset over the Northern Hemisphere based on the European Space Agency's GlobSnow project. [25]. However, the new GlobSnow product shows high uncertainties in Northeast China [9] and does not calculate the SWE in mountainous areas [26].

Although PMW remote sensing technology has advantages in the inversion of snow parameters, all existing SD products based on PWM have coarse spatial resolution, often tens of kilometers [27]. In addition, a complex nonlinear relationship also exists between the SD and surface environment parameters. It is difficult for existing SD products to achieve satisfactory accuracy [28], especially in Northeast China, which has complex environments. The interaction between rugged surface topography and atmospheric processes leads to significant spatial variability in snow properties. Measurements at a point are often non-representative of spatially averaged snow properties in mountainous areas [29,30]. Numerous researchers put forward various SD downscaling algorithms to enhance the spatial resolution of the existing SD products and inversion accuracy. For instance, Gao et al. [31] developed cloud-free snow cover data and then derived subpixel SWE data by combining the AMSR-E and MODIS systems. Mhawej et al. [32] used a weight factor based on snow cover duration to account for the statistical distribution of snow and obtained subpixel SWE data from AMSR-E SWE data. Yan et al. [33] obtained the downscaled SD data with 5 km $\times$ 5 km spatial resolution based on the snow cover probability model over the Tibetan Plateau. Although the spatial resolution of the existing SD or SWE products data had improved considerably compared with raw products, many studies have illustrated that complex environmental parameters could lead to large uncertainties in SD assessment [11,34]. Wang et al. [35] and Wei et al. [36] reconstructed SD data using PMW data and others related auxiliary data over the Tibetan Plateau, but the performance of their algorithms has not been validated in Northeast China.

The progress has been made in downscaling the existing SD or SWE product by taking advantage of high spatial resolution optical data, but owing to the complex nonlinear relationship between SD and surface parameters, few algorithms considered both the influence of spatial resolution and the complex environmental factors for SD inversion in high-latitude regions. Over the last decade, machine learning (ML) has achieved amazing success for evaluating surface characteristics based on remote sensing measurements data at both the local and global scales [37], and it has great potential in modeling the complex nonlinear relationships [38]. Therefore, in this study, a multifactor SD downscaling model that considers both the influence of spatial resolution and the complex environmental factors is developed based on a ML approach, which improved the accuracy while increasing the coarse spatial resolution of the existing SD products. First, we used a methodology to derive subpixel SD data by combining PMW SD product (25 km) and cloud-free snow cover product (500 m). Subsequently, environmental factors, including geolocation, topographical features, and land cover fraction were introduced, to reduce the impact of environmental factors on the accuracy of SD estimations, and eventually to develop a multifactor SD downscaling model that considers the influence of spatial resolution and the complex environmental factors in Northeast China.

In this paper, Section 2 presents the study area and data. The methodology for the development of the multifactor SD downscaling model is described in Section 3. The feasibility study of the multifactor SD downscaling model, the validation with observed SD datasets, and the comparison with existing general downscaling algorithms are demonstrated in Section 4. Potential affecting factors are discussed in Section 5. Finally, Section 6 induces the conclusions of the study.

2. Study Area and Data

2.1. Study Area

Northeast China (121.819°E–129.857°E, 47.745°N–53.175°N), as shown in Figure 1a, is one of the most important seasonal snow regions in the world, and it has abundant snow resources. In addition, it is one of the four black soil regions in the world, maintaining the global food supply [12]. Furthermore, the land cover types in Northeast China are complex, the forest cover fraction exceeds 40% of the total area, posing a serious challenge to the assessment of SD [39]. Many studies have discovered that variations in snow thickness in Northeast China can have a considerable impact on climate change during the last few decades [9,10]. As a result, reliable assessment of the SD in Northeast China is crucial for assessing hydrologic processes, crop production, and ecosystems.

2.2. Ground Observations

In this study, December to March is regarded as snow season in Northeast China. Three validation datasets are available for assessing the performance of the multifactor SD downscaling model and are briefly introduced in Table 1.

Table 1. Three ground observation datasets.

Named	Date	Number of Samples	Target
Ground meteorological stations	2013, 2015, 2017	24,000	Train model and test model performance (test1)
	2014, 2016, 2018	20,000	Temporal validation and analysis (test2)
Snow route1	2017.12–2018.03	60	Spatial validation and analysis (test3)
Snow route2	2017.12–2018.03	102	
Quadrat observation	2018.01.23	17	Fine-scale validation and analysis

2.2.1. Ground Meteorological Stations (Dataset 1)

Dataset 1 represents observed SD samples from ground meteorological stations during January 2013 to March 2018. There are 98 ground meteorological stations in Northeast China, as shown in Figure 1a, and they were obtained from the website at http://data.cma.cn/en (Accessed on 18 July 2019, National Meteorological Information Centre, China Meteorology Administration). A total of 24,000 independent SD observations were collected during the snow season in 2013, 2015, and 2017; they were applied to train and test the performance of the multifactor SD downscaling model. Furthermore, a total of 20,000 independent SD observations were collected during the snow season in 2014, 2016, and 2018; they were applied to estimate the accuracy of the proposed model in long time series.

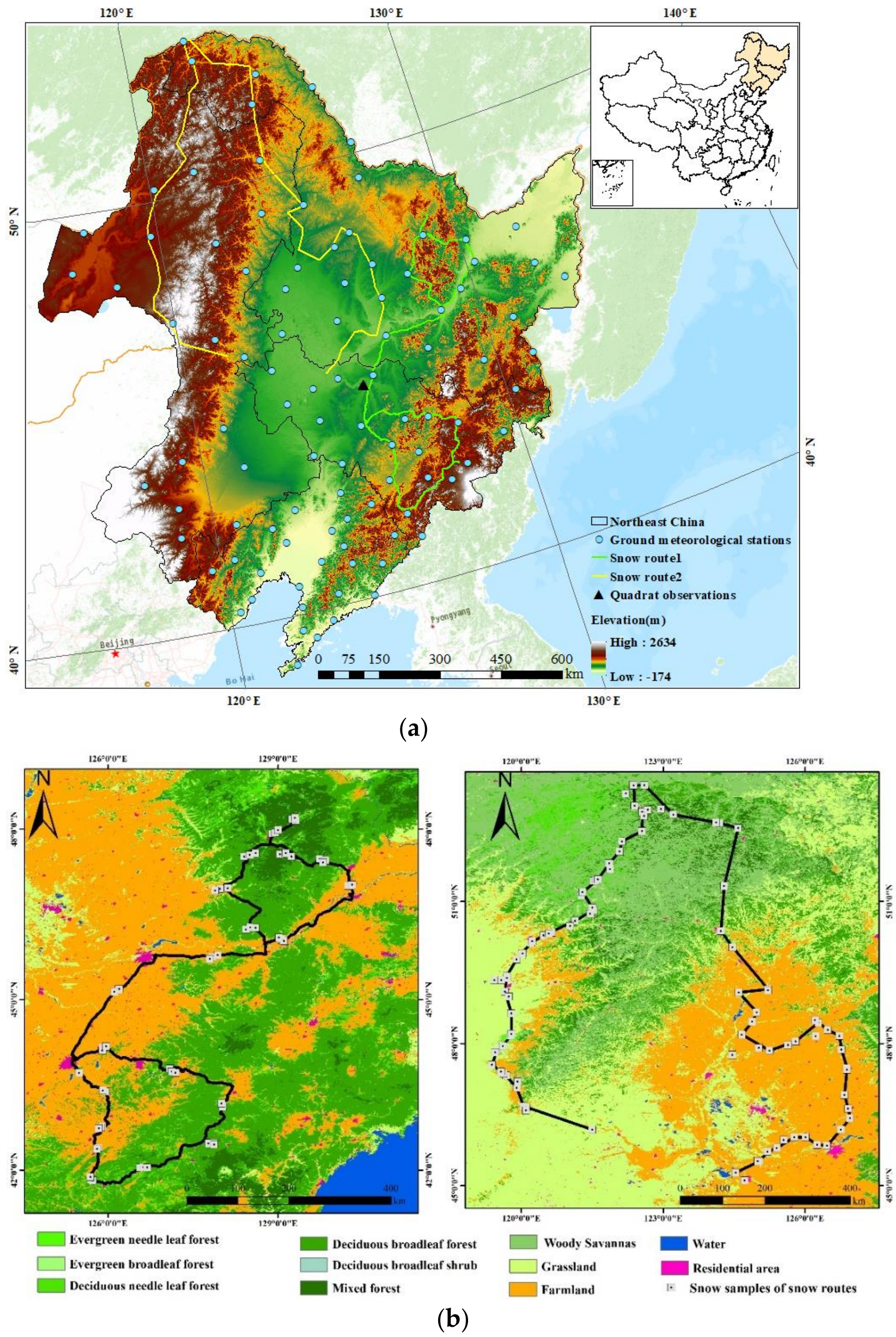

Figure 1. The study area is located in Northeast China. (**a**) The base map shows the elevation and spatial distribution of ground meteorological stations, the two colored lines are the field snow survey routes, and the black triangles represent snow observations within the quadrat. (**b**) Distributions of SD samples along two snow routes, respectively.

2.2.2. Snow Routes (Dataset 2)

Dataset 2 represents observed SD samples from field snow survey routes during December 2017 to March 2018, as shown in Figure 1b. The field snow survey experiment was supported by the Chinese snow survey project [25]. Snow route 1 was carried out in the Xiaoxing'an and Changbai Mountains, and a total of 60 snow samples were measured, which were mainly distributed in farmlands and forests. Snow route 2, which included 102 snow samples, was located in northern Inner Mongolia. The route was dominated by grassland and farmland. Dataset 2 was used to prove the applicability of the proposed model in space.

2.2.3. Observations within the Quadrat (Dataset 3)

Dataset 3 represents observed SD samples within grid cell. The black triangle in Figure 1a shows snow observation samples within the quadrat with a spatial resolution of 500 m, which were all distributed in farmland. There were 1–4 observations in each subpixel, and the geolocation, elevation (m), and SD (cm) were recorded. Observations within the quadrat help verify and analyze multifactor SD downscaling model in fine scale.

2.3. AMSR2 SD Product

The Advanced Microwave Scanning Radiometer 2 (AMSR2) instrument is a multifrequency (6, 7, 10, 18, 23, 36, and 89 GHz), dual-polarized (V, H) PMW radiometer launched in May 2012. Owing to the attenuation of snowpack caused by the microwave radiation from the snow and the underlying ground, the SD inversion algorithm based on AMSR2 brightness temperature data was developed by Kelly in 2009 [40]. Currently, the AMSR2 Level 3 SD product with the spatial resolution of the 25 km $\times$ 25 km has become the international mainstream SD product and can be downloaded from the site at https://gportal.jaxa.jp/gpr/ (Accessed on 22 August 2020). In this study, the descending SD products were acquired during snow seasons for avoiding the impact of snowmelt in daytime.

2.4. Daily Cloud-Free Snow Cover Data

In previous SD downscaling studies, it is necessary to establish the relationship between PMW SD data and optical snow cover extent data with high spatial resolution [41]. In this study, the daily cloud-free snow cover product with 500 m $\times$ 500 m resolution was acquired from the website at http://www.ncdc.ac.cn (Accessed on 22 August 2020) (the National Cryosphere Desert Data Center). The daily cloud-free snow cover product developed by Hao et al. [42], the optimal threshold of the Normalized Difference Snow Index (NDSI) was obtained for identifying snow cover under different land cover types, and snow cover extend could be identified more accurately. The snow cover days in each subpixel could be calculated based on the daily cloud-free snow cover data, which is a vital procedure for deriving subpixel SD in PMW pixels.

2.5. Vegetation Fraction Data

Previous research has shown that the land cover fraction has potential impact on SD inversion based on PMW brightness temperature data [38]. Therefore, the MODIS Vegetation Continuous Fields product (MOD44B) was used in this study, and which could be obtained from the website at https://search.earthdata.nasa.gov (Accessed on 22 August 2020). It describes the percentage of covered by tree canopy, nontree vegetation, and nonvegetation within a pixel with spatial resolution of 250 m. To match the cloud-free snow cover product, the original MOD44B data was mosaicked and resampled to 500 m.

2.6. DEM Data

The digital elevation model (DEM) data with 90 m $\times$ 90 m spatial resolution was obtained from the site at http://srtm.csi.cgiar.org (Accessed on 22 August 2020). First, the original DEM data were mosaicked, and resampled with the nearest-neighbor interpolation method to obtain elevation with a spatial resolution of 500 m. Subsequently, topographic factors (elevation, slope, aspect, and roughness) were calculated based on DEM data for eliminating the influence of topographic parameters on the SD inversion.

3. Methodology

3.1. Machine Learning Algorithms

Machine learning (ML) has the advantage of modeling the complex nonlinear relationships between the predictors and the response variable [43]. Three ML methods, including multiple linear regression (MLR), support vector regression (SVR), and random forest (RF), are assessed and compared in this study. They are implemented using the scikit-learn package in Python. The characteristics of each ML algorithm are summarized below.

MLR is used to describe the simultaneous associations of several variables with one continuous outcome. Many studies have shown that using MLR to construct the relationship between SD and surface parameters can obtain good prediction results in the Tibetan Plateau [35,36]. SVR is a class of supervised learning algorithms that have been widely used in solving nonlinear problems [44]. The kernel function in SVR is important for modeling complex nonlinear relationships. The linear kernel was adopted in this research. RF is an ensemble model based on decision trees, it was developed by Breiman in 2001 [45] and can make up a stronger predictor by composing the predictions from all weak learners (decision trees). Before employing the RF model, the number of decision trees in the ensemble (ntree) must typically be defined. In reference to Yang et al. [25], the values of the ntree is set to 1000 in this study. Futhermore, others system parameters in RF model are set to default.

3.2. Multifactor SD Downscaling Model Procedure

Many studies have revealed that there is a strong relationship between the snow cover duration and the SD during a given year [33,46]. Mhawej et al. [32] proposed a spatiotemporal weighting factor that accounts for the statistical distribution of snow cover duration to derive subpixel SD data within a PMW pixel. Since the snow cover data is available at a 500 m spatial resolution, each PMW pixel (25 km $\times$ 25 km) is overlaid by 2500 pixels representing the snow cover. Therefore, the subpixel SD data with 500 m $\times$ 500 m spatial resolution is obtained by the following expression:

$$\mathrm{SD}_{\mathrm{AMSR2\text{ - }SP}} = \begin{cases} 0, \text{ if the snow cover data has no snow} \\ \dfrac{\mathrm{SD}_{\mathrm{AMSR2}} \times 2500 \times \overline{\mathrm{SDT}}}{\mathrm{SDY}}, \text{ else} \end{cases} \tag{1}$$

where $\mathrm{SD}_{\mathrm{AMSR2}}$ is the raw AMSR2 SD product with a spatial resolution of 25 km $\times$ 25 km; $\overline{\mathrm{SDT}}$ is the average snow cover duration per year for each snow cover pixel (500 m $\times$ 500 m); and SDY is the sum of the total snow cover duration per year combined for each AMSR2 pixel. $\mathrm{SD}_{\mathrm{AMSR2\text{ - }SP}}$ presents the derived subpixel SD value (cm).

Many studies have also demonstrated that the accuracy of the PMW SD products is not only related to their coarse spatial resolution but also to the variations in complex environmental factors [34,35], which were considered in this study. The independent variables of geolocation variables, topographical features and land cover fraction factors are representative for expressing the complexity of a region [35,37], therefore, they were used in this study. Based on the ML method, a complex nonlinear relationship between SD and surface environmental factors can be developed. Thus, the multifactor SD downscaling model that considers both the influence of spatial resolution and complex environmental factors in Northeast China is expressed as follow:

$$\mathrm{D}_{\mathrm{AMSR2-SP}} = f(\mathrm{SD}_{\mathrm{AMSR2-SP}}, \text{Geolocation}, \text{Topographical features}, \text{Land cover fraction}) \tag{2}$$

where the geolocation variables included the longitude and latitude factors in each ground meteorological station; the topographical features included elevation, slope, aspect, and surface roughness; the land cover fraction factors included the percentage of the tree canopy, non-tree vegetation, and non-vegetation; f presents the ML methods; and $\mathrm{D}_{\mathrm{AMSR2-SP}}$ presents the downscaled SD value (cm) by the multifactor SD downscaling model. Figure 2 shows the multifactor SD downscaling model developed process as well as the evaluation of the procedure. The following steps explain the flowchart.

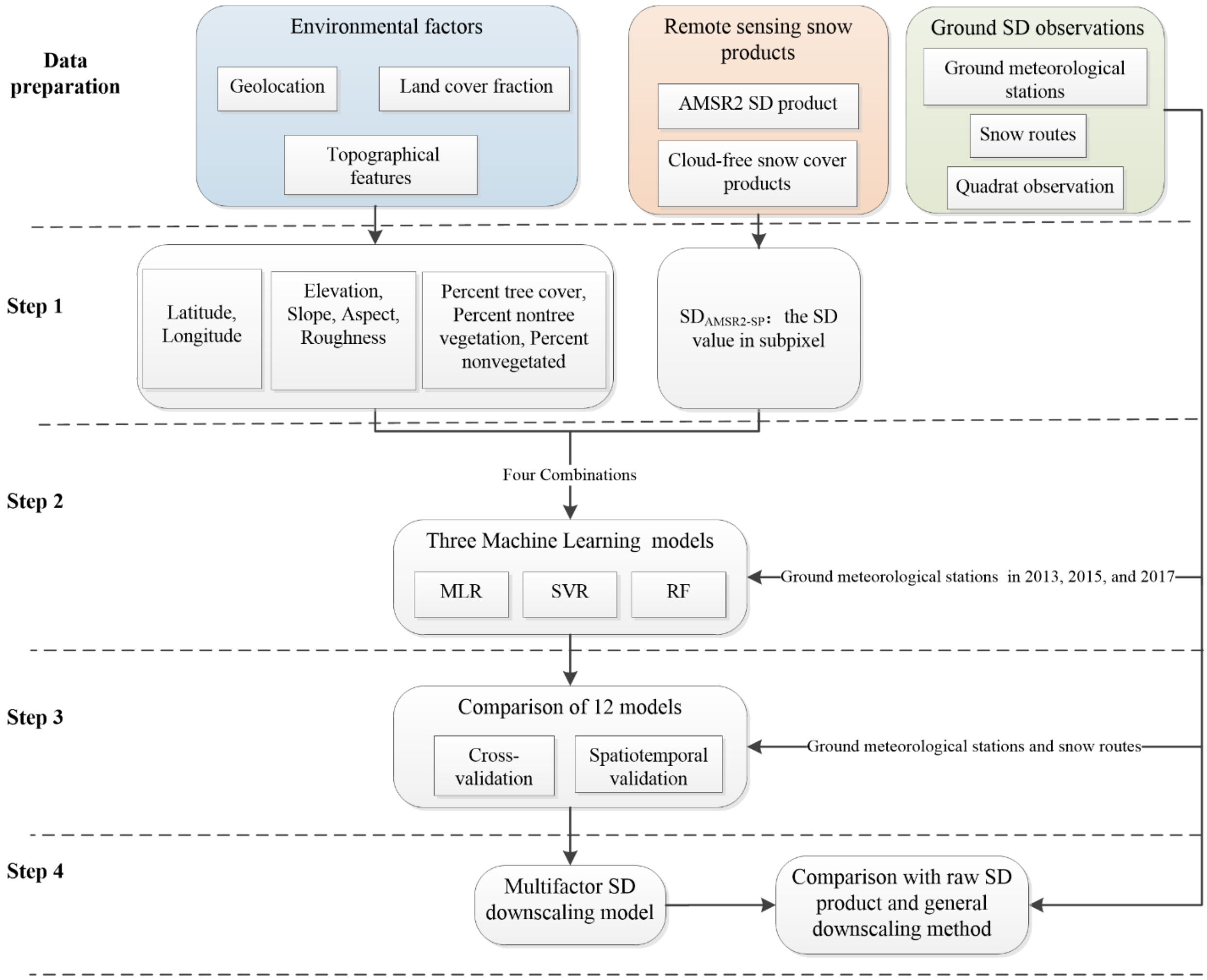

Figure 2. Flowchart of the multifactor SD downscaling model procedure.

Step 1: Selection of independent variables. As introduced in the above section, geolocation variables (latitude and longitude), topographical features (elevation, slope, aspect, and surface roughness), land cover fraction factors (the percentage of the tree canopy, non-tree vegetation, and non-vegetation), and $SD_{AMSR2-SP}$ data were used as input variables.

Step 2: Construction of the model. The multifactor SD downscaling model was constructed based on the ML. To determine a suitable model and selection rule for training samples during the regression, we selected three ML models, including MLR, SVR, and RF. For the selection rule, four combinations of independent variables were selected to train three ML models. Therefore, a total of 12 training models were generated in this study. Table 2 presents a detailed description of them.

Step 3: Model comparison. The performance of the 12 training models was comprehensively assessed. Using the same dataset for both model training and validation can produce over-optimistic assessments of model performance. The evaluation rule should ensure that the data used to verify models is distinct from the data used to train models. In this study, we applied 10-fold cross-validation (CV) strategies to test the performance of 12 regression models for SD inversion in Northeast China. We also implemented other SD observation data that are completely independent of the training dataset to provide a comprehensive comparison of the 12 regression models in time and space. The detailed results are shown in Table 2.

Table 2. A detailed error statistics of the 12 models based on three regression models with four combinations in three test datasets.

Name	Independent Variable	Regression Models	Test1 (10-Fold CV)			Test2 (Dataset 1)			Test3 (Dataset 2)			Note
			RMSE (cm)	BIAS (cm)	R	RMSE (cm)	BIAS (cm)	R	RMSE (cm)	BIAS (cm)	R	
M1	$SD_{AMSR2\text{-}SP}$	MLR	11.92	−0.03	0.35	8.05	−1.48	0.41	9.99	−3.73	0.38	Geolocation: lat, lon; Topographical features: Elevation, Slope, Aspect, Roughness; Land cover fraction: Percent_Tree_Cover, Percent_NonTree_ Vegetation, Percent_NonVegetated
		SVR	9.92	−1.01	0.36	8.01	−0.74	0.41	10.75	−8.31	0.36	
		RF	9.13	−0.16	0.38	8.04	−1.33	0.42	9.16	−2.24	0.41	
M2	$SD_{AMSR2\text{-}SP}$ + Geolocation	MLR	11.21	−0.11	0.39	8.03	−1.68	0.43	9.48	−3.63	0.44	
		SVR	9.47	−1.05	0.39	7.93	−0.84	0.43	10.40	−8.22	0.43	
		RF	7.24	0.08	0.64	7.75	−1.12	0.49	8.87	−1.42	0.48	
M3	$SD_{AMSR2\text{-}SP}$ + Geolocation + Topographical features	MLR	11.08	−0.02	0.42	7.83	−1.68	0.48	9.24	−3.61	0.45	
		SVR	9.20	−0.83	0.42	7.80	−1.06	0.48	10.14	−8.14	0.44	
		RF	7.32	0.17	0.68	7.58	1.15	0.53	8.63	−2.16	0.52	
M4	$SD_{AMSR2\text{-}SP}$ + Geolocation + Topographical features + Land cover fraction	MLR	10.98	−0.13	0.42	7.81	−1.78	0.48	9.31	−3.63	0.44	
		SVR	9.36	−0.60	0.43	7.86	−1.08	0.47	10.20	−8.26	0.43	
		RF	7.34	−0.03	0.69	7.58	−1.17	0.53	8.60	−2.18	0.52	

Step 4: Identification and validation of the best performance models. From the comparison results of the 12 models, we could select the model that exhibits the best performance and consider it as the final multifactor SD downscaling model. Then, the reconstructed SD data that considers both the influence of spatial resolution and the complex environmental factors was compared with the raw SD product and the general downscaling method. In addition, we applied quadrat observation data to analyze the performance of the multifactor SD downscaling model in fine scale. These detailed processes are found in Sections 4 and 5.

3.3. Accuracy Evaluation

We utilized a total of 24,000 observations selected from ground meteorological stations in 2013, 2015, and 2017 for training models and evaluated them using the 10-fold CV method. Subsequently, we implemented other SD observation data (20,000 samples) that were completely independent of the training dataset to provide a comprehensive comparison of the 12 regression models in time and space and finally determine the model that exhibits the best performance. The RMSE, Bias, and R were selected to evaluate the model accuracy in this paper, their criteria are as follows:

$$\mathrm{RMSE} = \sqrt{\sum_{i=1}^{N} (\mathrm{SD}_0 - \mathrm{SD}_x)^2 / N} \tag{3}$$

$$\mathrm{Bias} = \sum_{i=1}^{N} (\mathrm{SD}_0 - \mathrm{SD}_x) / N \tag{4}$$

$$R = \frac{\sum_{i=1}^{N} (\mathrm{SD}_0 - \overline{\mathrm{SD}_0})(\mathrm{SD}_x - \overline{\mathrm{SD}_x})}{\sqrt{\sum_{i=1}^{N} (\mathrm{SD}_0 - \overline{\mathrm{SD}_0})^2 \sum_{i=1}^{N} (\mathrm{SD}_x - \overline{\mathrm{SD}_x})^2}} \tag{5}$$

where SD_0 and SD_x represent the observed SD and the retrieved SD, respectively, and N is the number of samples used for evaluation.

4. Results

4.1. Selection of Optimal Models

Changing the number of input independent variables affects the regression model performance [47]. Comparing the validation results of four combinations (M1, M2, M3, and M4) in Table 2, we noticed that the overall accuracy of each regression model improved as the number of input independent variables increased. A notably decreased trend in the value of the RMSE for all models under the M1, M2, and M3 combinations was observed, as shown in Figure 3. The results showed that the spatiotemporal accuracy of SD inversion obviously improved when the geolocation factors and topographical features were considered. The M4 combination at Table 2, however, did not demonstrate that the regression model performs well as the number of input independent variables increases. The use of land cover fraction did not greatly affect the three regression models. The metrics shown in Table 2 indicated that the model performances in M4 exhibited a similar accuracy level compared with the validation results in M3. In summary, the independent variables in M3 were the most appropriate combination for the input of the regression model of this study.

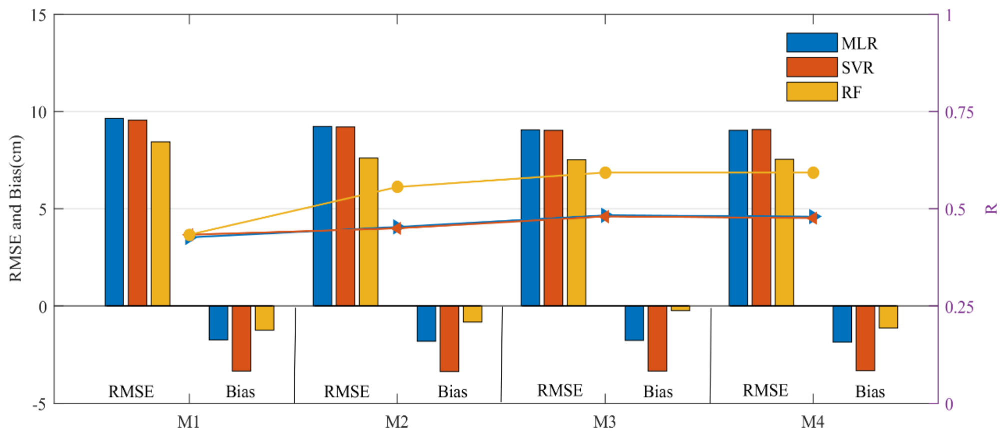

Figure 3. Comparison of the accuracy obtained with four different combinations across three regression models.

The three ML methods were able to produce a high correlation with ground observed SD in spatiotemporal prediction. As shown in Figure 3 shows, the R exceeds 0.3 for each ML model in four combinations. A detailed comparison results from Table 2, we could notice that the MLR and SVR regression model performed unsatisfactorily with four combinations using three validation datasets; it was more obvious in Figure 3 that the SVR and MLR regression model had a high value of RMSE in four combinations. The RF regression model considerably outperformed the other two regression models (MLR and SVR). Results demonstrated the potential of the RF-based regression model to represent the complex relationship between SD and other surface environmental factors. In addition, the good consistency between the retrieved SD and the observed SD confirmed that the proposed model can effectively describe SD spatial variations in fine scale. In general, the RF model proved to be the best regression model to train samples in this study. As shown in Table 2, the RF model in M3 had the highest SD inversion accuracy; its RMSE values were 7.32 cm, 7.58 cm, and 7.67 cm in three validation datasets (test1, test2, and test3), respectively. Finally, we selected the RF regression model in the M3 combination to construct a multifactor SD downscaling model, denoted as $D_{\mathrm{AMSR2-SP}}$.

4.2. Downscaling Results with the Multifactor SD Downscaling Model

While many studies indicated that it was difficult to discuss the fine-scale spatial variations of SD based on the PMW SD products, a significant advantage of the proposed multifactor SD downscaling model used in this study was that it considered the coarse spatial resolution of the PMW SD product. Figure 4(b1) shows the high-resolution SD distribution map (500 m $\times$ 500 m) based on the multifactor SD downscaling model on 23 January 2018 in Northeast China. The corresponding raw AMSR2 SD distribution map (25 km $\times$ 25 km) is demonstrated in Figure 4(a1). From a visual perspective, the SD maps exhibited similar spatial distribution patterns for both the high-resolution and coarse-resolution in Northeast China. The main difference between these two SD distribution maps was shown in the area surrounded by the red circle in Figure 4(a1,b1), with maximum and minimum differences of 30 and -5 cm, respectively. In addition, to test the performance of the multifactor SD downscaling model on a fine scale, a field quadrat (3 km × 2 km) observation experiment was designed on 23 January 2018 in Northeast China. As shown in Figure 4, the black triangles represent snow observation samples within the quadrat with a spatial resolution of 500 m. All snow observation samples were distributed in farmland, and a total of 17 grid cells were observed in this study. There were 1–4 SD observations per grid cell, and the observed SD within each grid cell were averaged to represent the ground truth SD. Figure 5 shows the comparison results between the retrieved SD and the observed SD. We conclude that the retrieved SD based on the multifactor SD downscaling model is in good agreement with the observed SD, and the error was distributed between −2 cm and 2 cm. The comparison results implied that the multifactor SD downscaling model could not only improve the raw PMW SD data spatial resolution but also better describe the subpixel spatial variations of SD (Figure 5), which is impossible for the existing PMW SD products.

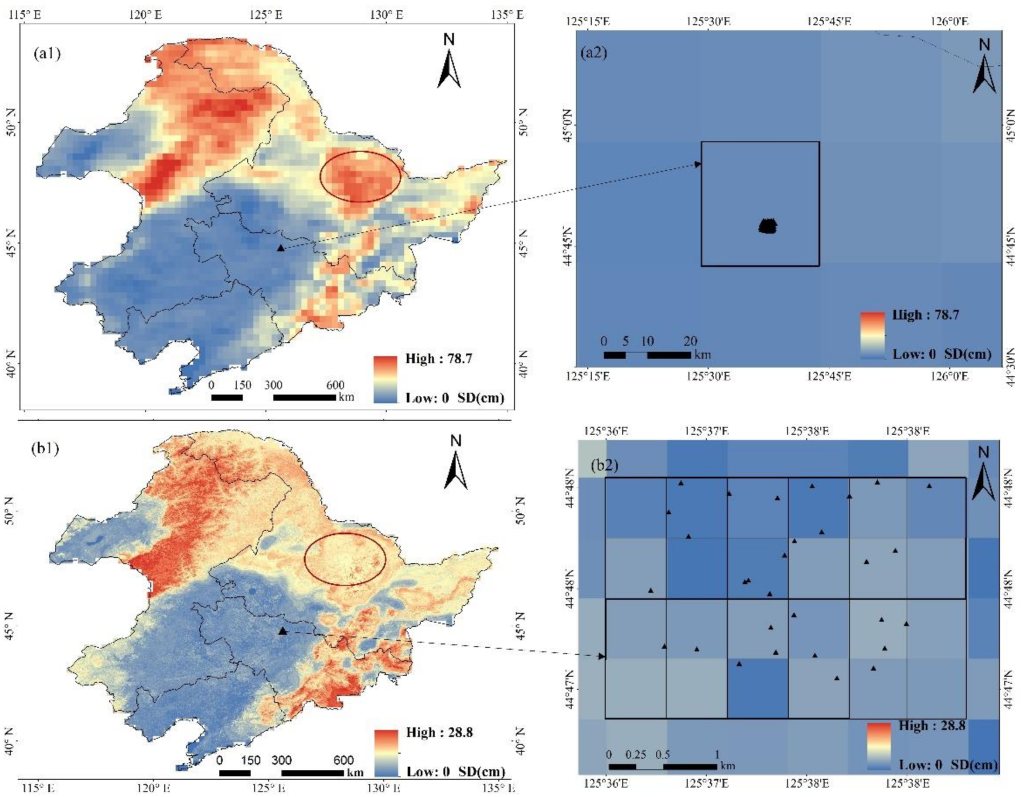

Figure 4. The SD spatial distribution on 23 January 2018 in Northeast China. (**a1**) AMSR2 (25 km × 25 km); (**b1**) D $_{\text{AMSR2-product}}$ (500 m × 500 m). (**a2**,**b2**) represent the corresponding SD map. The black triangles represent snow observations within the snow quadrat with a spatial resolution of 500 m.

4.3. Temporal Validation with Meteorological Station Dataset

The downscaled SD based on the multifactor SD downscaling model was evaluated using a ground meteorological station dataset during the snow season in 2014, 2016, and 2018. Meanwhile, to demonstrate the performance of the multifactor SD downscaling model, we also compared it with the general SD downscaling method in this study. As shown in Equation (6), the general SD downscaling model is based on the multifactor linear regression method that was proposed by Wei et al. in the Tibetan Plateau [36]. However, its performance had not been validated in Northeast China. Therefore, referring to the research of Wei et al. [36], the coefficients in Equation (6) in Northeast China were optimized and finally obtained the regression equation, as shown in Equation (7), denoted as the general SD downscaling model. Furthermore, to ensure a fair comparison between the raw AMSR2 SD products with coarse resolution and the downscaled SD data with finer scale, the raw AMSR2 SD product was resampled with a spatial resolution of 500 m × 500 m.

$$y = \beta_0 + \beta_1 X_1 + \beta_2 X_2 + \beta_3 X_3 + \ldots + \beta_i X_i + \mu \quad (6)$$

where y is the observed SD at the meteorological stations; X_1, X_2, X_3 X_i are snow characteristics and environmental factors; $\beta 0$, β_1, β_2, β_i are the model coefficients corresponding to the factors; μ is the error.

$$D_{\text{general}} = 5.43X_1 + 2.31X_2 - 1.12X_3 + 0.99X_4 - 0.89X_5 - 0.05X_6 + 0.59X_7 + 12.68 \quad (7)$$

where X_1–X_7 are the AMSR2 SD products (cm) with the spatial resolution of 500 m × 500 m, snow cover days (d), latitude (°), longitude (°), slope (°), roughness (cm), and elevation (m), respectively.

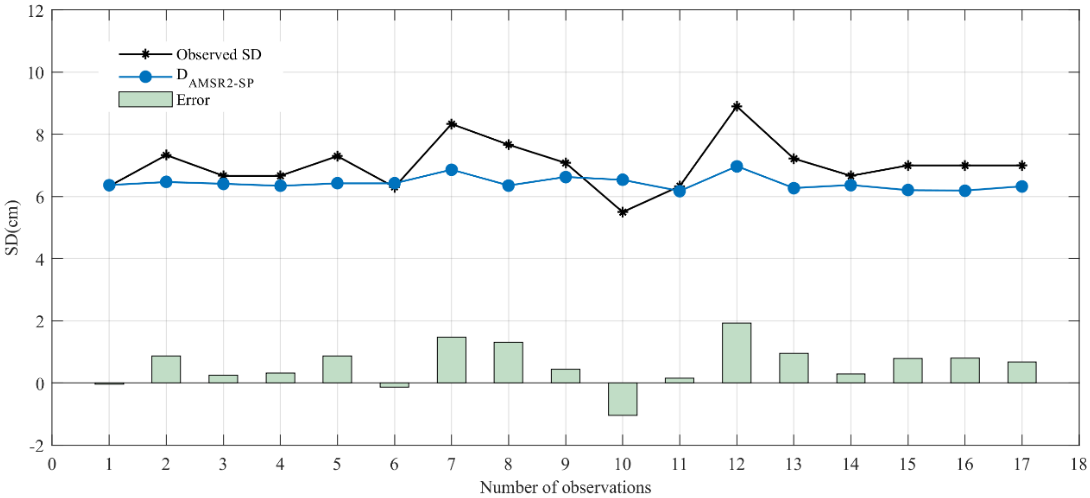

Figure 5. The comparison between $D_{\text{AMSR2-SP}}$ and the observed SD in the fine-scale.

Figure 6 shows the color density scatterplots of retrieved SD against observed SD for all investigated SD products. (a), (b), and (c) in Figure 6 represent the raw AMSR2 SD product, the downscaled SD based on Equation (7), and the downscaled SD based on proposed model in this study, respectively. The result of the raw AMSR2 SD product tends to be overestimated in terms of bias by 18 cm, with an RMSE of 26.15 cm (Figure 6a). Followed by the general SD downscaling model (Figure 6b), with the RMSE, bias, and R being 9.15 cm, 1.78 cm, and 0.40, respectively, the results showed that the general SD downscaling method can indeed improve the accuracy of the raw AMSR2 SD product in Northeast China. However, the multifactor SD downscaling model developed in this study achieved the best performance in terms of SD assessment. The RMSE decreased from 26.15 cm of the original product to 7.58 cm, whereas the R increased from 0.39 to 53. A more detailed overview of error statistics is presented in Table 3.

Table 3. Error statistics for the comparison between retrieved SD and observed SD in this study.

Snow Product	Dataset 1 (Temporal)			Dataset 2 (Spatial)		
	RMSE (cm)	Bias (cm)	R	RMSE (cm)	Bias (cm)	R
AMSR2	26.15	18.01	0.39	19.15	13.71	0.34
$D_{\text{general-AMSR2}}$	9.15	1.78	0.40	9.87	−2.63	0.36
$D_{\text{AMSR2-SP}}$	7.58	1.15	0.53	8.63	−2.16	0.52

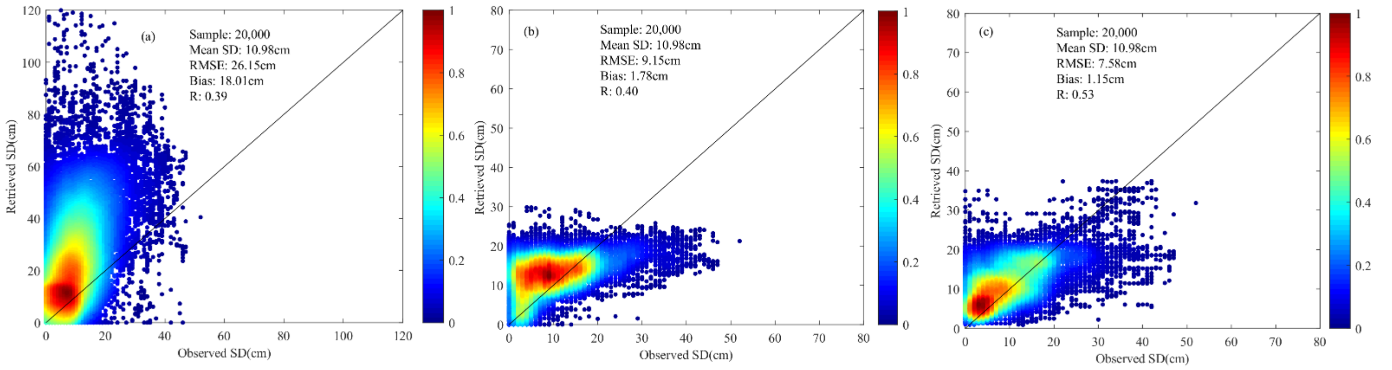

Figure 6. The color–density scatterplots of the retrieved SD and the observed SD at ground meteorological stations. (**a**–**c**) represent raw AMSR2 SD product, the downscaled SD based on general SD downscaling model, and the downscaled SD based on multifactor SD downscaling model, respectively.

4.4. Spatial Validation along the Snow Routes

Additionally, Figure 7 shows the scatter diagrams of the validation results against snow routes. Statistics results are listed in Table 3. The raw AMSR2 SD product seriously overestimated observed SD, having a bias of 13.71 cm, whereas the RMSE and R were 19.15 cm and 0.34, respectively. The general SD downscaling method based on Equation (7) could further improve the accuracy of the raw AMSR2 SD product in snow routes, as shown in Figure 7b, with the RMSE, bias, and R being 9.15 cm, 1.78 cm, and 0.40, respectively. Compared with the raw AMSR2 SD product and the general downscaling method, the corresponding downscaled SD based on the multifactor SD downscaling model demonstrated the best agreement with the in situ measurements, as shown in Figure 7c, with RMSE, Bias, and R being 8.63 cm, −2.16 cm, and 0.52, respectively. These results confirmed that the multifactor SD downscaling model that considers both the influence of spatial resolution and complex environmental factors was more reliable than the PMW SD.

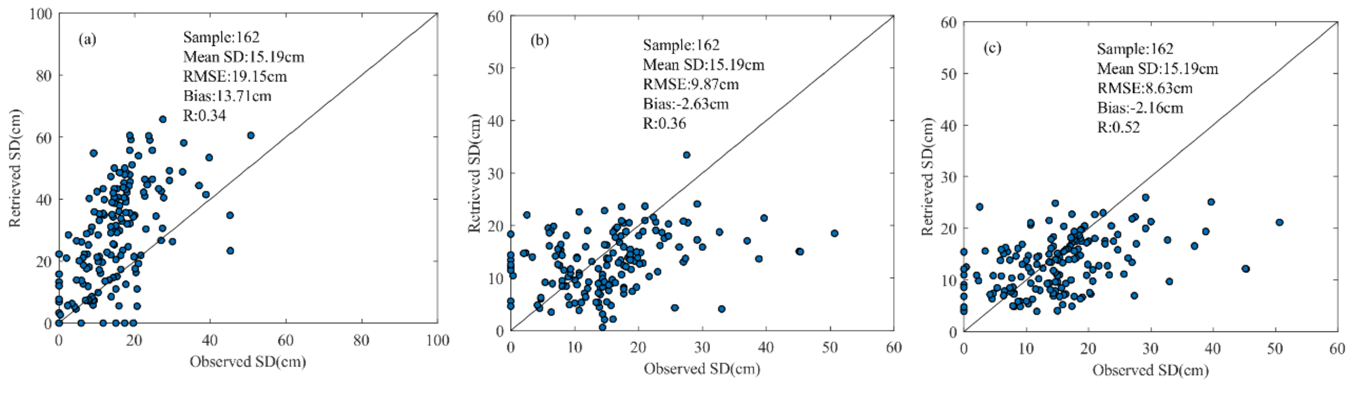

Figure 7. Scatter plots of retrieved SD and observed SD along the snow routes. (**a**–**c**) represent raw AMSR2 SD product, the downscaled SD based on general SD downscaling model, and the downscaled SD based on multifactor SD downscaling model, respectively.

5. Discussion

5.1. Regression Variable Importance

The estimation of the 12 models in Table 2 demonstrated that the remarkable performance of the RF-based regression method in revealing the complex nonlinear relationship between the observed SD and the surface environment parameters. The RF model can provide the importance of each input parameter in the process of the established regression model [25]. Figure 8 shows each variable's averaged importance scores derived from all input parameters and their corresponding maximum and minimum values based on the 10-fold CV error estimation. The results indicate that the inclusion of complex environmental variables has a very significant impact on the model performance. High scores can be found for $AMSR2_{SP}$ that were obtained by Equation (1). Its averaged importance scores exceeded 35. In addition, geographic location (latitude and longitude) help improve the multifactor SD downscaling model's spatiotemporal estimate. Compared with the prediction results in the M1 combination in Table 2, the SD inversion accuracy in the M2 combination significantly improved in time and space with the introduction of geographic information. Owing to the complex terrain in Northeast China (Figure 1a), the inclusion of topographical features (e.g., elevation, slope, aspect, and roughness) further improved the performance of the fitted models. The results in the M3 combination in Table 2 also indicated that the topographical features helped improve the accuracy of SD inversion. The land cover fraction weakly affected the accuracy of SD inversion; the maximum variable importance score of the land cover fraction is less than 5 (Figure 8). Therefore, the addition of land cover fraction does not significantly help for the performance of the proposed model. This also explains why the prediction accuracy in M5 combination in Table 2 did not further improve compared with the M4 combination in Table 2.

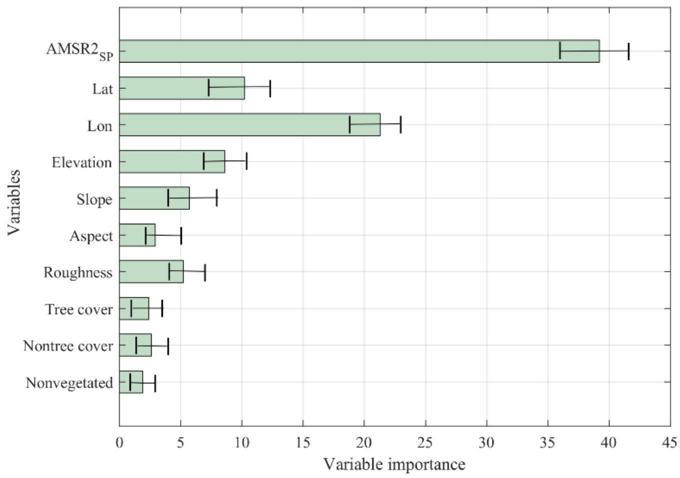

Figure 8. The ranking of variable importance for the RF-based multifactor SD downscaling model. The horizontal bars represent the variable importance scores.

5.2. Potential Errors of the Multifactor SD Downscaling Model

The accuracy of downscaled SD product is affected by the accuracy of original AMSR2 SD product. For a much coarser spatial resolution of AMSR2, the observed brightness temperature may contain various information, such as underlying frozen ground rather than snow properties, especially when the snowpack is shallow. Zhao et al. [48,49] have proposed a combined model to consider the effects from mixed pixels of frozen ground, snow and vegetation and the multilayer coherent effects from underlying soil layers. It was argued that frozen soil may present a similar microwave emission characteristic to snow, and uncertainties from frozen soil must be considered during the early stages of snowfall or late snowmelt.

Although high SD inversion accuracy was achieved using the multifactor SD downscaling model in most cases, Figure 9 indicated that the proposed model in this study still has potential errors for different observation SD. Overall, the RMSE values of the multifactor SD downscaling model increase as the SD increases. For deep snow (>30 cm), the multifactor SD downscaling model has bad inversion accuracy; its RMSE is up to 17.61 cm in Northeast China. This may be caused by saturation effects. The saturation effect of SD is difficult to overcome by using PMW data [38]. Figure 10 shows that the amount of deep snow was very small in the training datasets, which could explain why the model did not do well predicting deep snow. However, compared with the original

SD product and general downscaling model in Equation (7), the proposed model in this study still had the highest accuracy. We noticed that there was a slight overestimate of observed SD for all SD inversion models in shallow snow cover (SD < 10 cm), which may be attributed to the following reasons. First, the radiation signal from the snowpack is very weak for shallow snow, and the main source of the microwave energy is that from earth surface in such cases [50]. Second, frequent freeze–thaw cycles in the late snow season led to the growth of depth hoar in shallow snow [51], enhancing the scattering ability of the snowpack. As a result, the radiation signal was not close to the sensor. The brightness temperature difference was higher for shallow snowpack in this case, causing the model to overestimate the actual SD.

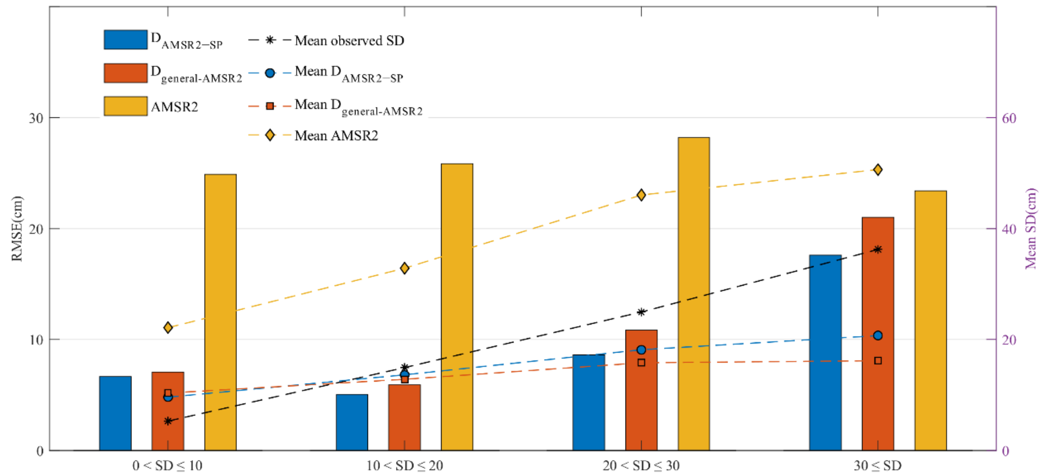

Figure 9. Statistical analysis results of the RMSE of the multifactor SD downscaling model based on the observed SD at ground meteorological stations. The corresponding dashed lines represent mean SD.

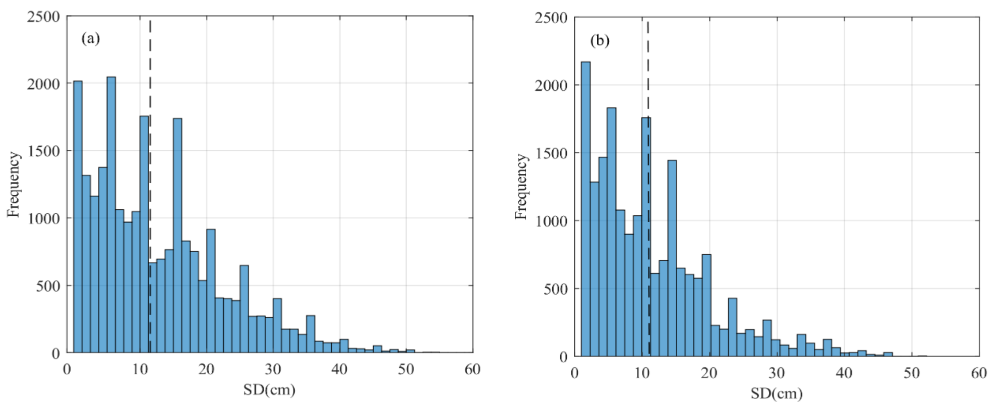

Figure 10. Histograms of SD observations from ground meteorological station dataset. (**a**) Training samples and (**b**) validation samples. The mean values (black dashed lines) are equal to 11.68 cm and 10.98 cm, respectively.

Figure 11 shows the impact of different snow seasons on the multifactor SD downscaling model. Overall, the monthly RMSE values of all SD assessment products and algorithms gradually increased with the date and peaked in March, which may be attributed to the following reasons. First, owing to the influence of snow cover metamorphism, snow grain size and snow density in the snowpack will rapidly grow with the snowfall period. For example, the snow grain size of new snow is less than 1 mm in December but more than 3 mm for old snow cover in March. Similarly, the snow density of new snow is less than 100 kg/m^3 in December, but more than 150 kg/m^3 for old snow cover in March [20]. The evolution of snow cover affects the accuracy of PMW SD products and then affects the downscaling model. Second, the impact of the liquid water content in the snowpack. We noticed in Figure 11 that the monthly mean observed SD gradually increased with the snowfall duration, reaching a maximum in February. However, the SD decreased in March, indicating that the snow began to melt at this time. PMW can interact with snow particles and detect the volume scattering signal of snowpack when snow is dry. The microwave signal changes dramatically owing to the increase of the liquid water fraction in the snowpack [52], causing great uncertainty for current SD products based on PMW signals, including our multifactor SD downscaling model.

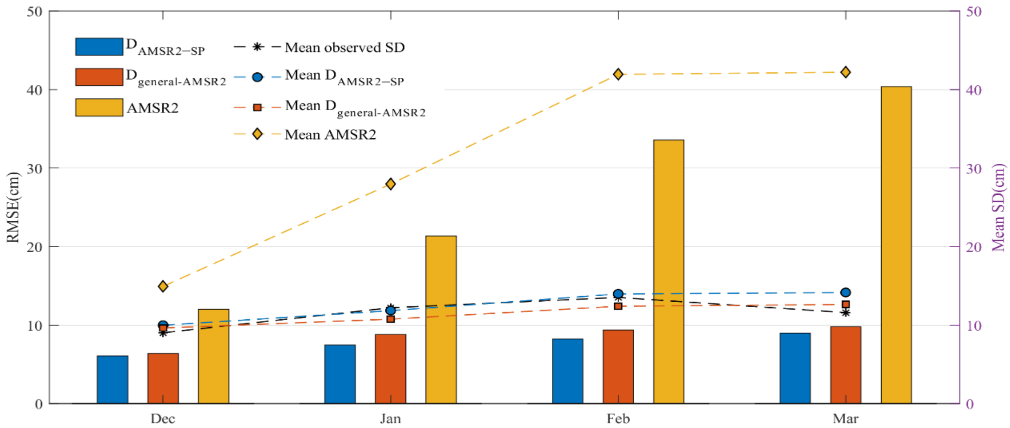

Figure 11. Monthly RMSE variations for the multifactor SD downscaling model. The corresponding dashed lines represent the monthly mean SD.

5.3. The Applicability of the Multifactor SD Downscaling Model in Other PMW SD Products

The multifactor SD downscaling model based on the AMSR2 SD product was evaluated in this study. However, different SD products demonstrated great spatiotemporal differences. Thus, it is important to demonstrate the applicability of the multifactor SD downscaling model in different SD products. Two additional PMW SD products, the WESTDC SD product and the FY SD product, were used to demonstrate the performance of the multifactor SD downscaling model for different SD products in time and space. The WESTDC algorithm modified the coefficient of the Chang algorithm using ground meteorological stations in China and introduced forest cover fractions to reduce the influence of forest canopy attenuation using a simple statistical method [16]. The WESTDC SD product can be obtained from the website at http://data.tpdc.ac.cn (Accessed on 22 August 2020). The FY algorithm considered the problem of land mixed pixels and atmospheric radiation [17]. For the snow distribution area of China, the daily FY SD dataset with a spatial resolution of 25 km from 1980 to 2020 was provided by the National Cryosphere Desert Data Center. (http://www.ncdc.ac.cn (Accessed on 22 August 2020)).

Figures 12 and 13 show that the raw WESTDC and FY products have better SD inversion accuracy in terms of time and space than the AMSR2 SD product in Northeast China. The FY SD product outperforms other operational satellite SD products considering the influence of atmospheric radiation and mixed pixels. However, the conventional SD inversion algorithms, including the WESTDC and FY products, are based on brightness temperature differences that make it difficult to overcome the influence of the coarse spatial resolution and complex surface parameters. We noticed that the proposed multifactor SD downscaling model in this study can further improve the WESTDC and the FY SD products in time and space and achieve better inversion accuracy than raw SD products (Table 4). The results in Table 4 illustrate that the multifactor SD downscaling model still has good applicability to other SD products. Therefore, it could be an effective method for addressing the large errors of existing PMW SD products in special complex environment areas in the future.

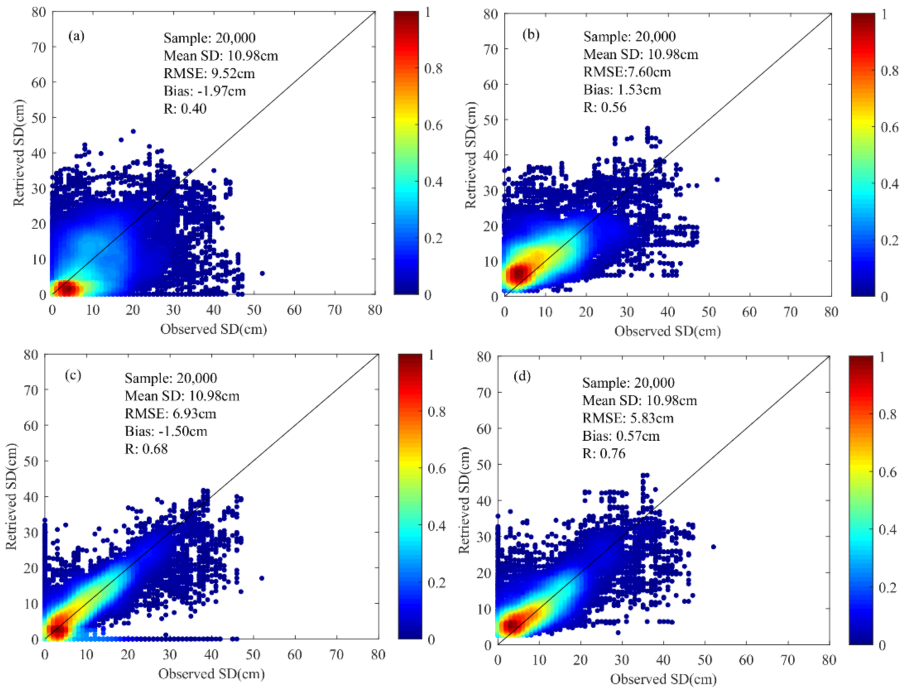

Figure 12. The color–density scatterplots of the retrieved SD and the observed SD at ground meteorological stations. (**a**,**c**) represent the raw WESTDC SD product and the FY SD product, respectively. (**b**,**d**) represent the corresponding downscaling results based on the multifactor SD downscaling model.

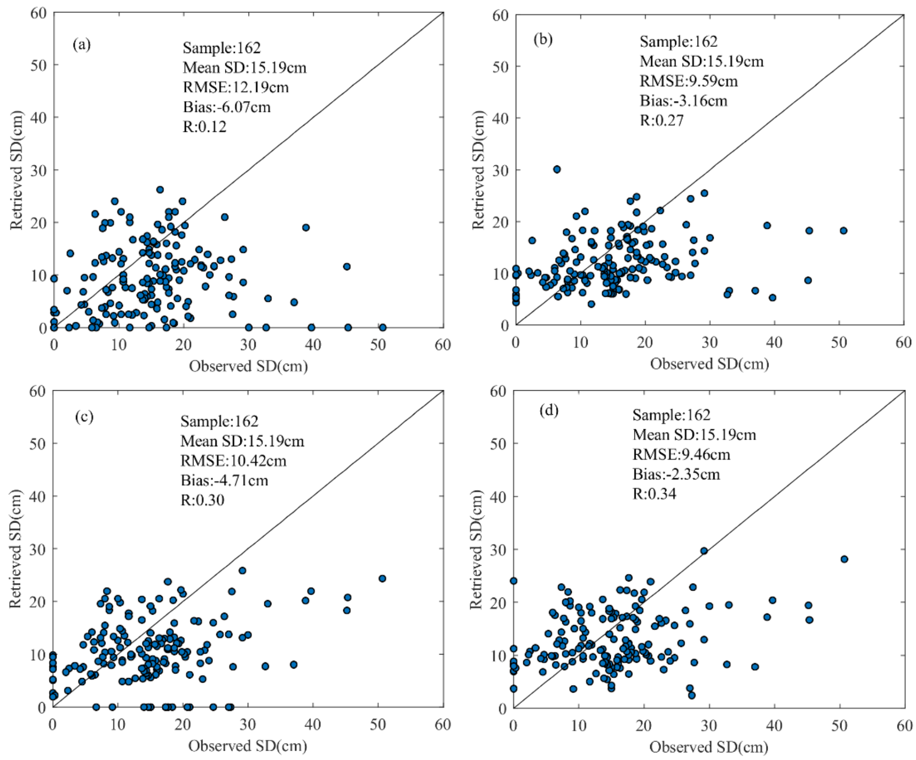

Figure 13. Scatter plots of retrieved SD and observed SD along the snow routes. (**a**,**c**) represent the raw WESTDC SD product and the FY SD product, respectively. (**b**,**d**) represent the corresponding downscaling results based on the multifactor SD downscaling model.

Table 4. Error statistics for the comparison between different SD products and observed SD in this study.

Snow Product	Dataset 1 (Temporal)			Dataset 2 (Spatial)		
	RMSE (cm)	Bias (cm)	R	RMSE (cm)	Bias (cm)	R
WESTDC	9.52	−1.97	0.40	12.19	−6.07	0.12
$D_{WESTDC\text{-}SP}$	7.60	1.53	0.56	9.59	−3.16	0.27
FY	6.93	−1.50	0.68	10.42	−4.71	0.30
$D_{FY\text{-}SP}$	5.83	0.57	0.76	9.46	−2.35	0.34

6. Conclusions

Accurate SD assessments are important in Northeast China for understanding crop production, climate change, and surface hydrological cycles. Currently, PMW remote sensing is the most effective method for SD monitoring in spatiotemporal variations. However, owing to the influence of coarse spatial resolution and complex environmental factors, the existing PMW SD products have large uncertainties, and it is difficult to accurately capture snow spatiotemporal variation. Therefore, we developed a multifactor SD downscaling model by combining AMSR2 PMW SD data, optical snow cover extent data, and surface environmental parameters to successfully downscale the PMW SD product at 25 km resolution to a higher resolution (500 m) and achieve satisfactory inversion accuracy. Through the analysis and verification in time and space, the main conclusions are as follows:

A total of 12 models were compared for illustrating the influence of different regression models and surface parameters and determining the optimal model as multifactor SD downscaling model. The results show that the introduction of surface parameter information indeed improved the performance of the regression models. The SD inversion spatiotemporal accuracy obviously improved when the geolocation factors and topographical features were considered, but the inclusion of land cover fraction did not effectively improve the performance in SD assessment. Moreover, the RF model-based regression method achieved the best performance compared with other ML regression methods including MLR and SVR.

The multifactor SD downscaling model that considers both the influence of spatial resolution and complex environmental factors achieved the best performance in terms of SD assessment in Northeast China when compared with the existing general downscaling methods. It could not only downscale the raw PMW SD product's spatial resolution but also improve their SD inversion accuracy. Furthermore, field quadrat (3 km $\times$ 2 km) observations shows that the proposed model is in good agreement with the observed SD, with the error ranging between −2 cm and 2 cm. Results demonstrated that the multifactor SD downscaling model can better describe the spatial variations of SD, which is impossible for raw PMW SD products.

In general, the multifactor SD downscaling model not only shows good spatial heterogeneity but also presents better temporal consistency against the observed SD from ground meteorological stations, thereby demonstrating strong potential for SD estimation. However, there are still challenges, such as underestimation for thicker snowpack, prior knowledge of snowpack (e.g., snow density and snow grain size), that should be considered to eliminate the potential error caused by snow cover evolution. In future work, we will attempt to construct a coupling system of ML and physical snow evolution model to overcome these shortcomings.

Author Contributions: Writing—original draft preparation, Y.W.; writing—review and editing, X.L. (Xiaofeng Li) and L.G.; visualization, X.Z. and L.L.; supervision, X.L. (Xiaojie Li) and T.J.; project administration, X.L. (Xiaofeng Li) and L.G.; funding acquisition, X.L. (Xiaofeng Li) and L.L. All authors have read and agreed to the published version of the manuscript.

Funding: This research was Supported by the Strategic Priority Research Program of the Chinese Academy of Sciences (Grant No. XDA28110502), National Natural Science Foundation of China

(41871248), Heilongjiang Provincial Natural Science Foundation of China (LH2020A023) and the Changchun Science and Technology Development Plan Project (No. 21ZY12).

Institutional Review Board Statement: Not applicable.

Informed Consent Statement: Not applicable.

Data Availability Statement: The data used to support the findings of this study are available from the corresponding author upon request.

Acknowledgments: The authors would like to thank the Science and Technology Basic Resources Survey Project of China for providing snow test data for this article.

Conflicts of Interest: The authors declare no conflict of interest.

References

1. Pulliainen, J.; Luojus, K.; Derksen, C.; Mudryk, L.; Lemmetyinen, J.; Salminen, M.; Ikonen, J.; Takala, M.; Cohen, J.; Smolander, T.; et al. Patterns and trends of Northern Hemisphere snow mass from 1980 to 2018. *Nature* **2020**, *581*, 294–298. [CrossRef] [PubMed]
2. Barnett, T.P.; Adam, J.C.; Lettenmaier, D.P. Potential impacts of a warming climate on water availability in snow-dominated regions. *Nature* **2005**, *438*, 303–309. [CrossRef] [PubMed]
3. Bormann, K.J.; Brown, R.D.; Derksen, C.; Painter, T.H. Estimating snow-cover trends from space. *Nat. Clim. Change* **2018**, *8*, 924–928. [CrossRef]
4. Henderson, G.R.; Peings, Y.; Furtado, J.C.; Kushner, P.J. Snow–atmosphere coupling in the Northern Hemisphere. *Nat. Clim. Change* **2018**, *8*, 954–963. [CrossRef]
5. Foster, J.L.; Chang, A.T.C.; Hall, D.K. Comparison of snow mass estimates from a prototype passive microwave snow algorithm, a revised algorithm and a snow depth climatology. *Remote Sens. Environ.* **1997**, *62*, 132–142. [CrossRef]
6. Cohen, J.; Entekhabi, D. Eurasian snow cover variability and northern hemisphere climate predictability. *Geophys. Res. Lett.* **1999**, *26*, 345–348. [CrossRef]
7. Pulliainen, J. Mapping of snow water equivalent and snow depth in boreal and sub-arctic zones by assimilating space-borne microwave radiometer data and ground-based observations. *Remote Sens. Environ.* **2006**, *101*, 257–269. [CrossRef]
8. Derksen, C.; Toose, P.; Rees, A.; Wang, L.; English, M.; Walker, A.; Sturm, M. Development of a tundra-specific snow water equivalent retrieval algorithm for satellite passive microwave data. *Remote Sens. Environ.* **2010**, *114*, 1699–1709. [CrossRef]
9. Che, T.; Dai, L.; Zheng, X.; Li, X.; Zhao, K. Estimation of snow depth from passive microwave brightness temperature data in forest regions of northeast China. *Remote Sens. Environ.* **2016**, *183*, 334–349. [CrossRef]
10. Gu, L.; Fan, X.; Li, X.; Wei, Y. Snow depth retrieval in farmland based on a statistical lookup table from passive microwave data in northeast China. *Remote Sens.* **2019**, *11*, 3037. [CrossRef]
11. Li, X.; Zhao, K.; Wu, L.; Zheng, X.; Jiang, T. Spatiotemporal analysis of snow depth inversion based on the FengYun-3B MicroWave radiation imager: A case study in Heilongjiang Province, China. *J. Appl. Remote Sens.* **2014**, *8*, 084692. [CrossRef]
12. Liang, S.; Li, X.; Zheng, X.; Jiang, T.; Li, X.; Qiao, D. Effects of winter snow cover on spring soil moisture based on remote sensing data product over farmland in Northeast China. *Remote Sens.* **2020**, *12*, 2716. [CrossRef]
13. Chang, A.T.C.; Foster, J.L.; Hall, D.K. Nimbus-7 SMMR Derived Global Snow Cover Parameters. *Ann. Glaciol.* **1987**, *9*, 39–44. [CrossRef]
14. Kopczynski, S.; Ramage, J.M.; Lawson, D.E.; Goetz, S.; Evenson, E.B.; Denner, J.; Larson, G. Passive microwave (SSM/I) satellite predictions of valley glacier hydrology, Matanuska Glacier, Alaska. *Geophys. Res. Lett.* **2008**, *35*, 034615. [CrossRef]
15. Mätzler, C.; Wiesmann, A. Extension of the Microwave Emission Model of Layered Snowpacks to Coarse-Grained Snow. *Remote Sens. Environ.* **1999**, *70*, 317–325. [CrossRef]
16. Tao, C.; Xin, L.; Rui, J.; Armstrong, R.; Zhang, T. Snow depth derived from passive microwave remote-sensing data in China. *Ann. Glaciol.* **2008**, *49*, 145–154.
17. Yang, J.; Jiang, L.; Wu, S.; Wang, G.; Wang, J.; Liu, X. Development of a Snow Depth Estimation Algorithm over China for the FY-3D/MWRI. *Remote Sens.* **2019**, *11*, 977. [CrossRef]
18. Kelly, R.E.; Chang, A.T.; Tsang, L.; Foster, J.L. A prototype AMSR-E global snow area and snow depth algorithm. *IEEE Trans. Geosci. Remote Sens.* **2003**, *41*, 230–242. [CrossRef]
19. Dai, L.; Che, T.; Wang, J.; Zhang, P. Snow depth and snow water equivalent estimation from AMSR-E data based on a priori snow characteristics in Xinjiang, China. *Remote Sens. Environ.* **2012**, *127*, 14–29. [CrossRef]
20. Wei, Y.; Li, X.; Gu, L.; Zheng, M.X.; Jiang, T.; Li, X.; Wan, X. A Dynamic Snow Depth Inversion Algorithm Derived from AMSR2 Passive Microwave Brightness Temperature Data and Snow Characteristics in Northeast China. *IEEE J. Sel. Top. Appl. Earth Obs. Remote Sens.* **2021**, *14*, 5123–5136. [CrossRef]
21. Pulliainen, J.T.; Grandell, J.; Hallikainen, M.T. HUT snow emission model and its applicability to snow water equivalent retrieval. *IEEE Trans. Geosci. Remote Sens.* **1999**, *37*, 1378–1390. [CrossRef]

22. Tan, S.; Chang, W.; Tsang, L.; Lemmetyinen, J.; Proksch, M. Modeling Both Active and Passive Microwave Remote Sensing of Snow Using Dense Media Radiative Transfer (DMRT) Theory With Multiple Scattering and Backscattering Enhancement. *IEEE J. Sel. Top. Appl. Earth Obs. Remote Sens.* **2015**, *8*, 4418–4430. [CrossRef]
23. Santi, E.; Pettinato, S.; Paloscia, S.; Pampaloni, P.; Fontanelli, G.; Crepaz, A.; Valt, M. Monitoring of Alpine snow using satellite radiometers and artificial neural networks. *Remote Sens. Environ.* **2014**, *144*, 179–186. [CrossRef]
24. Du, J.; Kimball, J.S.; Jones, L.A.; Kim, Y.; Glassy, J.; Watts, J.D. A global satellite environmental data record derived from AMSR-E and AMSR2 microwave Earth observations. *Earth Syst. Sci. Data* **2017**, *9*, 791–808. [CrossRef]
25. Yang, J.W.; Jiang, L.M.; Lemmetyinen, J.; Luojus, K.; Takala, M.; Wu, S.L.; Pan, J.M. Validation of remotely sensed estimates of snow water equivalent using multiple reference datasets from the middle and high latitudes of China. *J. Hydrol.* **2020**, *590*, 125499. [CrossRef]
26. Li, D.; Durand, M.; Margulis, S.A. Potential for hydrologic characterization of deep mountain snowpack via passive microwave remote sensing in the Kern River basin, Sierra Nevada, USA. *Remote Sens. Environ.* **2012**, *125*, 34–48. [CrossRef]
27. Gu, L.; Ren, R.; Li, X. Snow Depth Retrieval Based on a Multifrequency Dual-Polarized Passive Microwave Unmixing Method From Mixed Forest Observations. *IEEE Trans. Geosci. Remote Sens.* **2016**, *54*, 7279–7291. [CrossRef]
28. Yang, J.; Jiang, L.; Luojus, K.; Pan, J.; Lemmetyinen, J.; Takala, M.; Wu, S. Snow depth estimation and historical data reconstruction over China based on a random forest machine learning approach. *Cryosphere* **2020**, *14*, 1763–1778. [CrossRef]
29. Molotch, N.P.; Bales, R.C. Scaling snow observations from the point to the grid element: Implications for observation network design. *Water Resour. Res.* **2005**, *41*, 1–17. [CrossRef]
30. Slater, A.G.; Barrett, A.P.; Clark, M.P.; Lundquist, J.D.; Raleigh, M.S. Uncertainty in seasonal snow reconstruction: Relative impacts of model forcing and image availability. *Adv. Water Resour.* **2013**, *55*, 165–177. [CrossRef]
31. Yang, G.; Xie, H.; Lu, N.; Tandong, Y.; Tiangang, L. Toward advanced daily cloud-free snow cover and snow-water equivalent products from Terra-Aqua MODIS and Aqua AMSR-E measurements. *J. Hydrol.* **2010**, *385*, 23–35.
32. Mhawej, M.; Faour, G.; Fayad, A.; Shaban, A. Towards an enhanced method to map snow cover areas and derive snow-water equivalent in Lebanon. *J. Hydrol.* **2014**, *513*, 274–282. [CrossRef]
33. Yan, D.; Ma, N.; Zhang, Y. Development of a fine-resolution snow depth product based on the snow cover probability for the Tibetan Plateau: Validation and spatial–temporal analyses. *J. Hydrol.* **2021**, *604*, 127027. [CrossRef]
34. Yang, J.W.; Jiang, L.M.; Lemmetyinen, J.; Pan, J.M.; Luojus, K.; Takala, M. Improving snow depth estimation by coupling HUT-optimized effective snow grain size parameters with the random forest approach. *Remote Sens. Environ.* **2021**, *264*, 112630. [CrossRef]
35. Wang, Y.; Huang, X.; Wang, J.; Zhou, M.; Liang, T. AMSR2 snow depth downscaling algorithm based on a multifactor approach over the Tibetan Plateau, China. *Remote Sens. Environ.* **2019**, *231*, 111268. [CrossRef]
36. Wei, P.; Zhang, T.; Zhou, X.; Yi, G.; Li, J.; Wang, N.; Wen, B. Reconstruction of snow depth data at moderate spatial resolution (1 km) from remotely sensed snow data and multiple optimized environmental factors: A case study over the qinghai-tibetan plateau. *Remote Sens.* **2021**, *13*, 657. [CrossRef]
37. Bair, E.H.; Calfa, A.A.; Rittger, K.; Dozier, J. Using machine learning for real-time estimates of snow water equivalent in the watersheds of Afghanistan. *Cryosphere* **2018**, *12*, 1579–1594. [CrossRef]
38. Xiao, X.; Zhang, T.; Zhong, X.; Shao, W.; Li, X. Support vector regression snow-depth retrieval algorithm using passive microwave remote sensing data. *Remote Sens. Environ.* **2018**, *210*, 48–64. [CrossRef]
39. Guangrui, W.; Xiaofeng, L.; Xiuxue, C.; Tao, J.; Xingming, Z.; Yanlin, W.; Xiangkun, W.; Jian, W. An investigation on microwave transmissivity at frequencies of 18.7 and 36.5 GHz for diverse forest types during snow season. *Int. J. Digit. Earth* **2021**, *14*, 1354–1379. [CrossRef]
40. Kelly, R. The AMSR-E Snow Depth Algorithm: Description and Initial Results. *J. Remote Sens. Soc. Jpn.* **2009**, *29*, 307–317.
41. Zhu, L.; Zhang, Y.; Wang, J.; Tian, W.; Liu, Q.; Ma, G.; Kan, X.; Chu, Y. Downscaling snow depth mapping by fusion of microwave and optical remote-sensing data based on deep learning. *Remote Sens.* **2021**, *13*, 584. [CrossRef]
42. Hao, X.; Huang, G.; Che, T.; Ji, W.; Sun, X.; Zhao, Q.; Zhao, H.; Wang, J.; Li, H.; Yang, Q. The NIEER AVHRR snow cover extent product over China—A long-term daily snow record for regional climate research. *Earth Syst. Sci. Data* **2021**, *13*, 4711–4726. [CrossRef]
43. Wu, Y.; Duguay, C.R.; Xu, L. Assessment of machine learning classifiers for global lake ice cover mapping from MODIS TOA reflectance data. *Remote Sens. Environ.* **2021**, *253*, 112206. [CrossRef]
44. Mountrakis, G.; Im, J.; Ogole, C. Support vector machines in remote sensing: A review. *ISPRS J. Photogramm. Remote Sens.* **2011**, *66*, 247–259. [CrossRef]
45. Breiman, L. Random forests. *Mach. Learn.* **2001**, *45*, 5–32. [CrossRef]
46. Dai, L.; Che, T.; Xie, H.; Wu, X. Estimation of Snow Depth over the Qinghai-Tibetan Plateau Based on AMSR-E and MODIS Data. *Remote Sens.* **2018**, *10*, 1989. [CrossRef]
47. Wei, Z.; Sanchez, N.; Hui, L.; Ainong, L. A spatial downscaling approach for the SMAP passive surface soil moisture product using random forest regression. *J. Hydrol.* **2018**, *563*, 1009–1024.
48. Zhao, T.; Zhang, L.; Jiang, L.; Zhao, S.; Chai, L.; Jin, R. A new soil freeze/thaw discriminant algorithm using AMSR-E passive microwave imagery. *Hydrol. Processes* **2011**, *25*, 1704–1716. [CrossRef]

49. Zhao, T.; Shi, J.; Zhao, S.; Chen, K.; Wang, P.; Li, S.; Xiong, C.; Xiao, Q. Measurement and Modeling of Multi-Frequency Microwave Emission of Soil Freezing and Thawing Processes. In Proceedings of the 2018 Progress in Electromagnetics Research Symposium (PIERS-Toyama), Toyama, Japan, 1–4 August 2018.
50. Gu, L.; Ren, R.; Li, X.; Zhao, K. Snow Depth Retrieval Based on a Multifrequency Passive Microwave Unmixing Method for Saline-Alkaline Land in the Western Jilin Province of China. *IEEE J. Sel. Top. Appl. Earth Obs. Remote Sens.* **2018**, *11*, 2210–2222. [CrossRef]
51. Dai, L.; Che, T.; Ding, Y.; Hao, X. Evaluation of snow cover and snow depth on the Qinghai-Tibetan Plateau derived from passive microwave remote sensing. *Cryosphere* **2017**, *11*, 1933–1948. [CrossRef]
52. Markus, T.; Powell, D.C.; Wang, J.R. Sensitivity of passive microwave snow depth retrievals to weather effects and snow evolution. *IEEE Trans. Geosci. Remote Sens.* **2006**, *44*, 68–77. [CrossRef]